RadioGraphics

Fatty Liver: Imaging Patterns and Pitfalls[1]

Okka W. Hamer, MD • Diego A. Aguirre, MD • Giovanna Casola, MD
Joel E. Lavine, MD • Matthias Woenckhaus, MD • Claude B. Sirlin, MD

ONLINE-ONLY CME

See www.rsna.org/education/rg_cme.html.

LEARNING OBJECTIVES

After reading this article and taking the test, the reader will be able to:

- Recognize the imaging features of fat accumulation in the liver.
- Describe the possible causes of fat accumulation in the liver.
- Differentiate fat accumulation in the liver from malignant and benign mimics.

TEACHING POINTS

See last page

Fat accumulation is one of the most common abnormalities of the liver depicted on cross-sectional images. Common patterns include diffuse fat accumulation, diffuse fat accumulation with focal sparing, and focal fat accumulation in an otherwise normal liver. Unusual patterns that may cause diagnostic confusion by mimicking neoplastic, inflammatory, or vascular conditions include multinodular and perivascular accumulation. All of these patterns involve the heterogeneous or nonuniform distribution of fat. To help prevent diagnostic errors and guide appropriate work-up and management, radiologists should be aware of the different patterns of fat accumulation in the liver, especially as they are depicted at ultrasonography, computed tomography, and magnetic resonance imaging. In addition, knowledge of the risk factors and the pathophysiologic, histologic, and epidemiologic features of fat accumulation may be useful for avoiding diagnostic pitfalls and planning an appropriate work-up in difficult cases.

Abbreviation: GRE = gradient echo

RadioGraphics 2006; 26:1637–1653 • **Published online** 10.1148/rg.266065004 • **Content Code:** GI

[1]From the Departments of Diagnostic Radiology (O.W.H.) and Pathology (M.W.), University Hospital of Regensburg, Regensburg, Germany; Department of Radiology, Fundación Santa Fe de Bogotá, University Hospital, Bogotá, Colombia (D.A.A.); and Departments of Radiology (G.C., C.B.S.) and Pediatrics (J.E.L.), UCSD Medical Center San Diego, 200 W Arbor Dr, San Diego, CA 92103. Recipient of a Certificate of Merit award for an education exhibit at the 2004 RSNA Annual Meeting. Received January 20, 2006; revision requested March 6; revision received April 20; accepted May 4. All authors have no financial relationships to disclose. **Address correspondence to** C.B.S. (e-mail: *csirlin@ucsd.edu*).

Conditions Associated with Fatty Liver

Most Common	Common	Rare	Congenital
Alcohol overuse	Viral infection	Nutritional or dietary abnormality	Monogenic disorders
Insulin resistance	Hepatitis C	Total parenteral nutrition	Metabolic disorders
Obesity	Hepatitis B	Rapid weight loss	Fatty oxidation defect
Hyperlipidemia	Drug use	Starvation	Organic aciduria
	Steroids	Surgery (eg, jejuno-ileal bypass)	Aminoacidopathy
	Chemotherapeutic agents	Iatrogenic injury	Storage disorders
	Amiodarone	Radiation therapy	Glycogen storage disorder
	Valproic acid		α_1-Antitrypsin deficiency
			Wilson disease
			Hemochromatosis
			Other
			Cystic fibrosis
			Dysmorphic syndromes associated with obesity
			Bardet-Bridel
			Prader-Willy

Introduction

Fatty liver is a common abnormality among patients undergoing cross-sectional imaging of the abdomen. The image-based diagnosis of fatty liver usually is straightforward, but fat accumulation may be manifested with unusual structural patterns that mimic neoplastic, inflammatory, or vascular conditions. On these occasions, the imaging appearance of the liver may cause diagnostic confusion and lead to unnecessary diagnostic tests and invasive procedures. To avoid such mistakes, radiologists should be aware of the many imaging manifestations of fatty liver. This article provides a review of the risk factors and the pathophysiologic, histologic, epidemiologic, and imaging appearances of fat accumulation in the liver. The authors describe the different structural patterns of fat accumulation that may be seen at ultrasonography (US), computed tomography (CT), and magnetic resonance (MR) imaging. They also discuss diagnostic pitfalls and explain how to distinguish between fat deposition and more ominous conditions of the liver.

Teaching Point

Risk Factors and Pathophysiologic Features

Fatty liver is a term applied to a wide spectrum of conditions characterized histologically by triglyceride accumulation within the cytoplasm of hepatocytes. The two most common conditions associated with fatty liver are alcoholic liver disease and nonalcoholic fatty liver disease. Alcoholic liver disease is caused by excess alcohol consumption, whereas the nonalcoholic variant is related to insulin resistance and the metabolic syndrome. Other relatively common conditions associated with fat accumulation in the liver include viral hepatitis and the use or overuse of certain drugs. Rarer associated conditions include dietary and nutritional abnormalities and congenital disorders (Table).

These conditions all cause a triglyceride accumulation (steatosis) within hepatocytes by altering the hepatocellular lipid metabolism, in particular, by causing defects in free fatty acid metabolic pathways (1–6). Hepatocytes in the center of the lobule (near the central vein) are particularly vulnerable to metabolic stress and tend to accumulate lipid earlier than those in the periphery (1,7). Consequently, in many of these conditions, steatosis tends to be most pronounced histologically in the zone around the central veins and less pronounced in zones around the portal triads. In advanced cases, there is diffuse, relatively homogeneous involvement of the entire lobule (7).

In many conditions associated with fatty liver, steatosis may progress to steatohepatitis (with inflammation, cell injury, or fibrosis accompanying steatosis) and then cirrhosis (7–10). However, because progression to steatohepatitis is uncommon, a "two-hit" model has been proposed. The "first hit" is the cytoplasmic deposition of triglycerides in hepatocytes, which may make the hepatocytes more vulnerable to a "second hit" but

Figure 1. Normal appearance of the liver at US. The echogenicity of the liver is equal to or slightly greater than that of the renal cortex *(rc)*.

Figure 2. Normal appearance of the liver at unenhanced CT. The attenuation of the liver (66 HU) is slightly higher than that of the spleen (56 HU), and intrahepatic vessels *(v)* appear hypoattenuated in comparison with the liver.

which, in the absence of the second hit, does not lead to progressive disease. The second hit has not yet been identified but is thought to represent a constellation of superimposed cellular events that promote inflammation and cell injury and incite progression to fibrosis and cirrhosis. In support of the two-hit model, there are data that suggest that the coexistence of steatosis with other liver diseases, such as viral hepatitis, increases the risk of disease progression (4).

In the radiology literature, the term *fatty infiltration of the liver* is often used to describe fat deposition. Despite its common use, the term is misleading because fat deposition is characterized histologically by the accumulation of discrete triglyceride droplets in hepatocytes and, rarely, in other cell types. Infiltration of fat into the parenchyma does not occur. The term *fatty liver* is more accurate and therefore is used in this article.

To grade steatosis, pathologists visually estimate the fraction of hepatocytes that contain fat droplets. Typically, a five-point ordinal scale is used (0%, 1%–5%, 6%–33%, 34%–66%, ≥67%). The size of fat droplets is not considered (7).

Prevalence of Fatty Liver

The prevalence of fatty liver in the general population is about 15%, but it is higher among those who consume large quantities (>60 g per day) of alcohol (45%), those with hyperlipidemia (50%) or obesity (body mass index, >30 kg/m^2) (75%), and those with both obesity and high alcohol consumption (95%) (4,11–16).

Imaging-based Diagnosis of Fatty Liver

Liver biopsy and histologic analysis is considered the diagnostic reference standard for the assessment of fatty liver. However, fatty liver also can be diagnosed with the use of cross-sectional imaging.

Diagnosis at US

The echogenicity of the normal liver equals or minimally exceeds that of the renal cortex or spleen. Intrahepatic vessels are sharply demarcated, and posterior aspects of the liver are well depicted (Fig 1). Fatty liver may be diagnosed if liver echogenicity exceeds that of renal cortex and spleen and there is attenuation of the ultrasound wave, loss of definition of the diaphragm, and poor delineation of the intrahepatic architecture (17–21). To avoid false-positive interpretations, fatty liver should not be considered present if only one or two of these criteria are fulfilled.

Teaching Point

Diagnosis at CT

At unenhanced CT, the normal liver has slightly greater attenuation than the spleen and blood, and intrahepatic vessels are visible as relatively hypoattenuated structures (Fig 2). Fatty liver can be diagnosed if the attenuation of the liver is at least 10 HU less than that of the spleen (17,22,23) or if the attenuation of the liver is less than 40 HU (24–26). In severe cases of fatty liver, intrahepatic vessels may appear hyperattenuated relative to the fat-containing liver tissue (17). Other CT criteria

Teaching Point

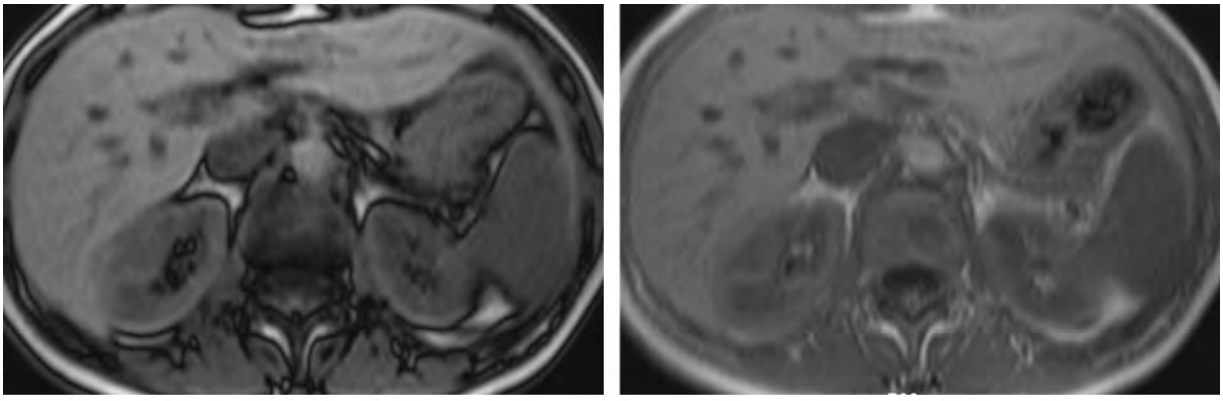

a. b.

Figure 3. Normal appearance of the liver at MR imaging. Axial opposed-phase **(a)** and axial in-phase **(b)** T1-weighted GRE images show similar signal intensity of the liver parenchyma.

have been advocated. Ricci et al, for example, measured the liver-to-spleen attenuation ratio and interpreted a ratio of less than 1 as indicative of fatty liver (27). This group also quantified liver fat by performing unenhanced CT in conjunction with dedicated fat calibration phantoms.

At contrast material–enhanced CT, the comparison of liver and spleen attenuation values is not as reliable for the diagnosis of fatty liver, because differences between the appearance of the liver and that of the spleen depend on timing and technique and because there is overlap between normal and abnormal attenuation value ranges (28,29). Fatty liver can be diagnosed at contrast-enhanced CT if absolute attenuation is less than 40 HU, but this threshold has limited sensitivity.

Diagnosis at MR Imaging

Chemical shift gradient-echo (GRE) imaging with in-phase and opposed-phase acquisitions is the most widely used MR imaging technique for the assessment of fatty liver. The signal intensity of the normal liver parenchyma is similar on in-phase and opposed-phase images (Fig 3). Fatty liver may be present if there is a signal intensity loss on opposed-phase images in comparison with in-phase images (30–33), and the amount of hepatic fat present can be quantified by assessing the degree of signal intensity loss (34).

Teaching Point

Fat deposition also can be diagnosed by observing the signal intensity loss of liver on MR images after the application of chemical fat saturation sequences, but this method is less sensitive than is chemical shift GRE imaging for the detection of fatty liver.

On in-phase GRE images or T1- or T2-weighted echo-train spin-echo images, higher than normal liver signal intensity is suggestive of fat deposition, but this finding is neither sensitive nor specific (30–32,35,36) unless the measurement technique is correctly calibrated.

Proton MR spectroscopy is the most accurate noninvasive method for the assessment of fatty liver (37–39). However, this method does not generate anatomic images, and a discussion of it is therefore beyond the scope of this article.

Accuracy for Detection and Grading of Fat Deposition

Reported sensitivities and specificities for detection of fatty liver deposition are 60%–100% and 77%–95% for US (4,17,19), 43%–95% and 90% for unenhanced CT (40), and 81% and 100% for chemical shift GRE MR imaging (31). A US-, CT-, and MR imaging–based diagnosis of fatty liver may be unreliable in the presence of a liver fat content of less than 30% in wet weight (19, 23), although MR techniques that are currently in developmental stages are likely to be reliable even in the presence of a low liver fat content.

A few research groups have developed CT and MR techniques that show promise for use in the quantitative grading of liver fat content (27,31,34,37).

Patterns of Fat Deposition

Diffuse Deposition

Diffuse fat deposition in the liver is the most frequently encountered pattern. Liver involvement usually is homogeneous, and the image interpretation is straightforward if the rules specified earlier are applied (Figs 4–6).

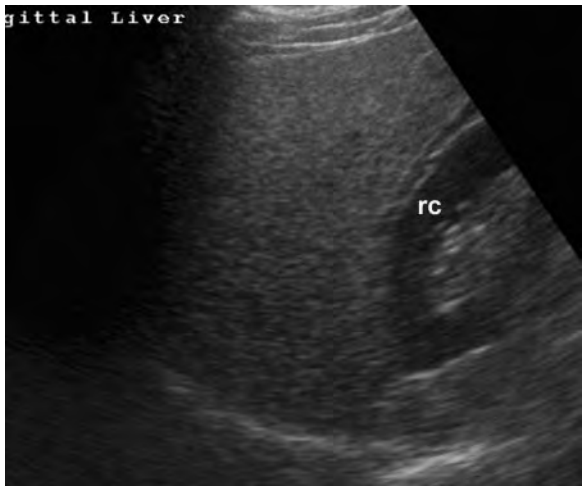

Figure 4. Diffuse fat accumulation in the liver at US. The echogenicity of the liver is greater than that of the renal cortex *(rc)*. Intrahepatic vessels are not well depicted. The ultrasound beam is attenuated posteriorly, and the diaphragm is poorly delineated.

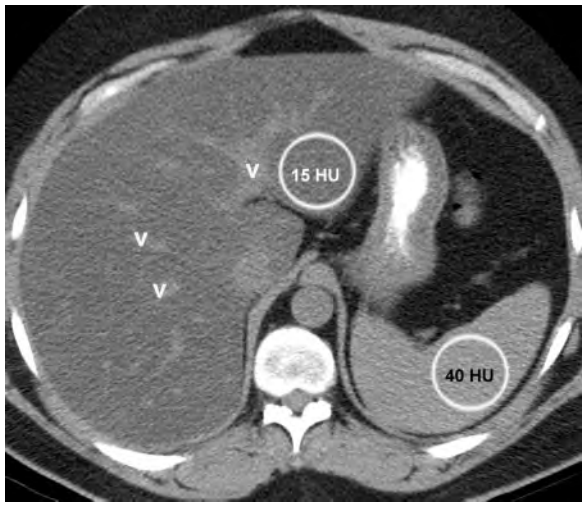

Figure 5. Diffuse fat accumulation in the liver at unenhanced CT. The attenuation of the liver (15 HU) is markedly lower than that of the spleen (40 HU). Intrahepatic vessels *(v)* also appear hyperattenuated in comparison with the liver.

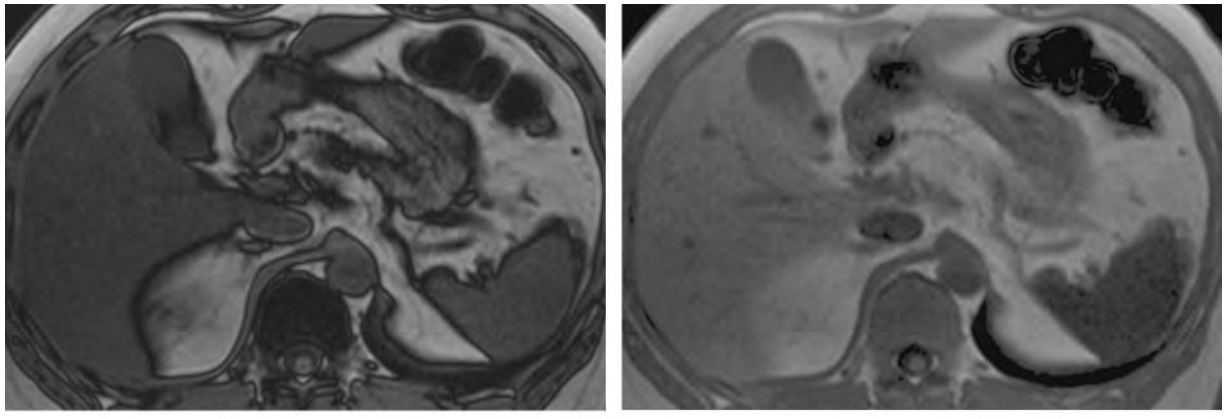

a. **b.**

Figure 6. Diffuse fat accumulation in the liver at MR imaging. Axial T1-weighted GRE images show a marked decrease in the signal intensity of the liver on the opposed-phase image **(a)**, compared with that on the in-phase image **(b)**.

Focal Deposition and Focal Sparing

Slightly less common patterns are focal fat deposition and diffuse fat deposition with focal sparing. In these patterns, focal fat deposition or focal fat sparing characteristically occurs in specific areas (eg, adjacent to the falciform ligament or ligamentum venosum, in the porta hepatis, and in the gallbladder fossa) (41–46); this distribution is not yet fully understood but has been attributed to variant venous circulation, such as anomalous gastric venous drainage (41,44). Focal fat deposition adjacent to insulinoma metastases also has been reported and is thought to be due to local insulin effects on hepatocyte triglyceride synthesis and accumulation (47–49).

The diagnosis of focal fat deposition and focal sparing is more difficult than that of homogeneously diffuse fat deposition because imaging findings may resemble mass lesions. Imaging findings suggestive of fatty pseudolesions rather than true masses include the following: fat content, location in areas characteristic of fat deposition or sparing, absence of a mass effect on vessels and other liver structures, a geographic configuration rather than a round or oval shape, poorly delineated margins, and contrast enhancement that is similar to or less than that of the normal liver parenchyma.

Teaching Point

Figure 7. Focal fat accumulation in the liver at US. Transverse image shows, adjacent to the left portal vein, a geographically shaped area of high echogenicity that represents accumulation of fat *(f)* in the falciform ligament, with posterior acoustic attenuation (arrows).

Figure 8. Focal fat accumulation in the liver at CT. Axial contrast-enhanced image obtained during the portal venous phase shows hypoattenuated regions of focal fat accumulation adjacent to the falciform and venous ligaments and in the porta hepatis, with no evidence of a mass effect.

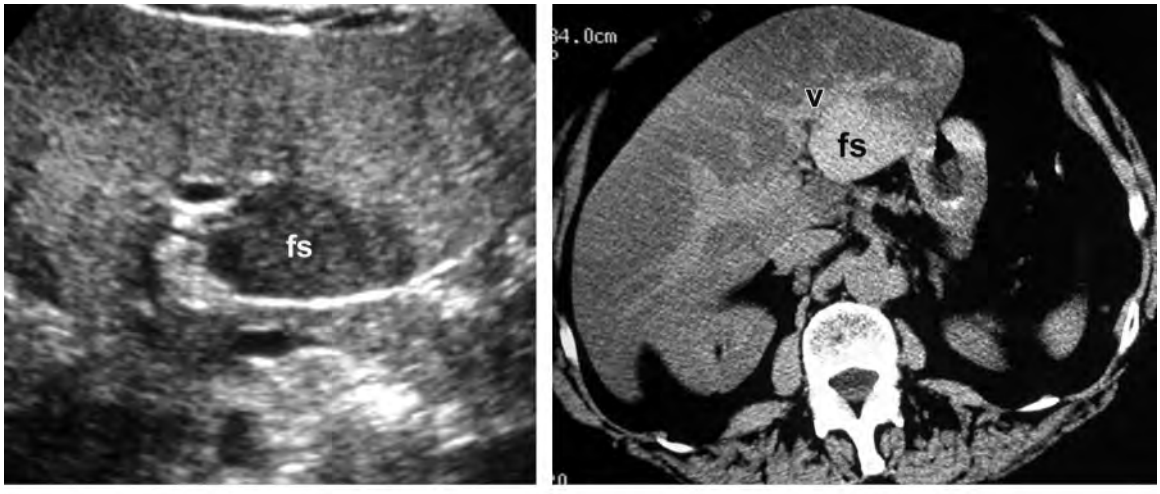

a. **b.**

Figure 9. Diffuse fat accumulation with focal sparing at US and CT. Transverse US image **(a)** and axial unenhanced CT image **(b)** obtained at comparable levels show high echogenicity and hypoattenuation, respectively, features indicative of a diffuse accumulation of fat in the liver. Focal sparing *(fs)* is manifested as a geographically shaped area with relative hypoechogenicity in **a** and hyperattenuation in **b**. The focal fatty pseudolesion exerts no mass effect on the adjacent vessel (*v* in **b**).

Involved areas usually are relatively small, but occasionally there may be confluent heterogeneous regions of focal deposition and sparing that span large areas of the liver (Figs 7–9).

Multifocal Deposition

An uncommon pattern is multifocal fat deposition. In this pattern, multiple fat foci are scattered in atypical locations throughout the liver (Fig 10) (50–52). The foci may be round or oval and closely mimic true nodules. Correct diagnosis is

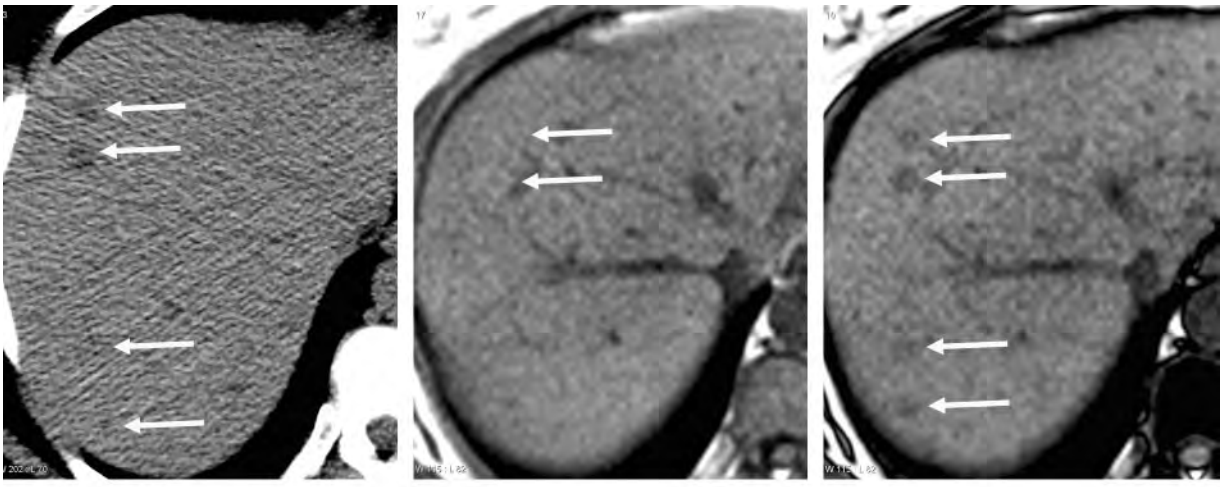

a. b. c.

Figure 10. Multifocal fat accumulation in the liver at CT and MR imaging in a 48-year-old woman with breast cancer. **(a)** Unenhanced CT image shows multiple hypoattenuated 1-cm nodules (arrows). **(b, c)** T1-weighted GRE MR images show nodules (arrows) with a signal intensity slightly higher than that of the normal liver parenchyma on the in-phase image **(b)** but with a signal intensity loss on the opposed-phase image **(c)**. The nodules were mistaken for metastases at CT but were correctly diagnosed as multifocal fat accumulation in the liver on the basis of MR findings.

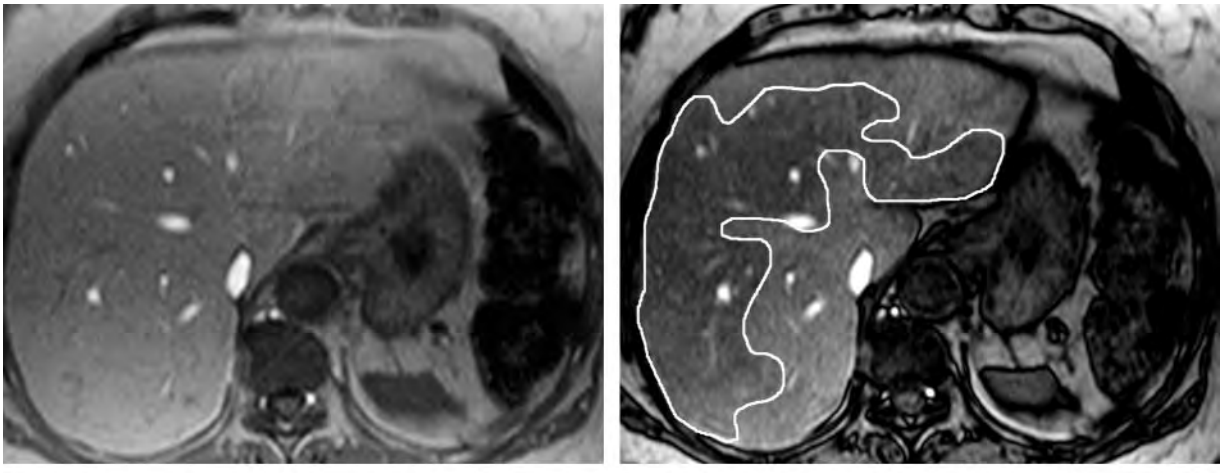

a. b.

Figure 11. Confluent foci of fat accumulation in the liver at MR imaging. Axial T1-weighted MR images show a large irregular region with a loss of signal intensity on the opposed-phase image (contour outline in **b**), compared with the signal intensity on the in-phase image **(a)**. Note the absence of a mass effect.

difficult, especially in patients with a known malignancy, and requires the detection of microscopic fat within the lesion. For this purpose, chemical shift GRE imaging is more reliable than CT or US. Other clues indicative of multifocal fat deposition are lack of a mass effect, stability in size over time, and contrast enhancement similar to or less than that in the surrounding liver parenchyma. In some cases, the foci of fat deposition have a confluent pattern (Fig 11). Multifocal fat

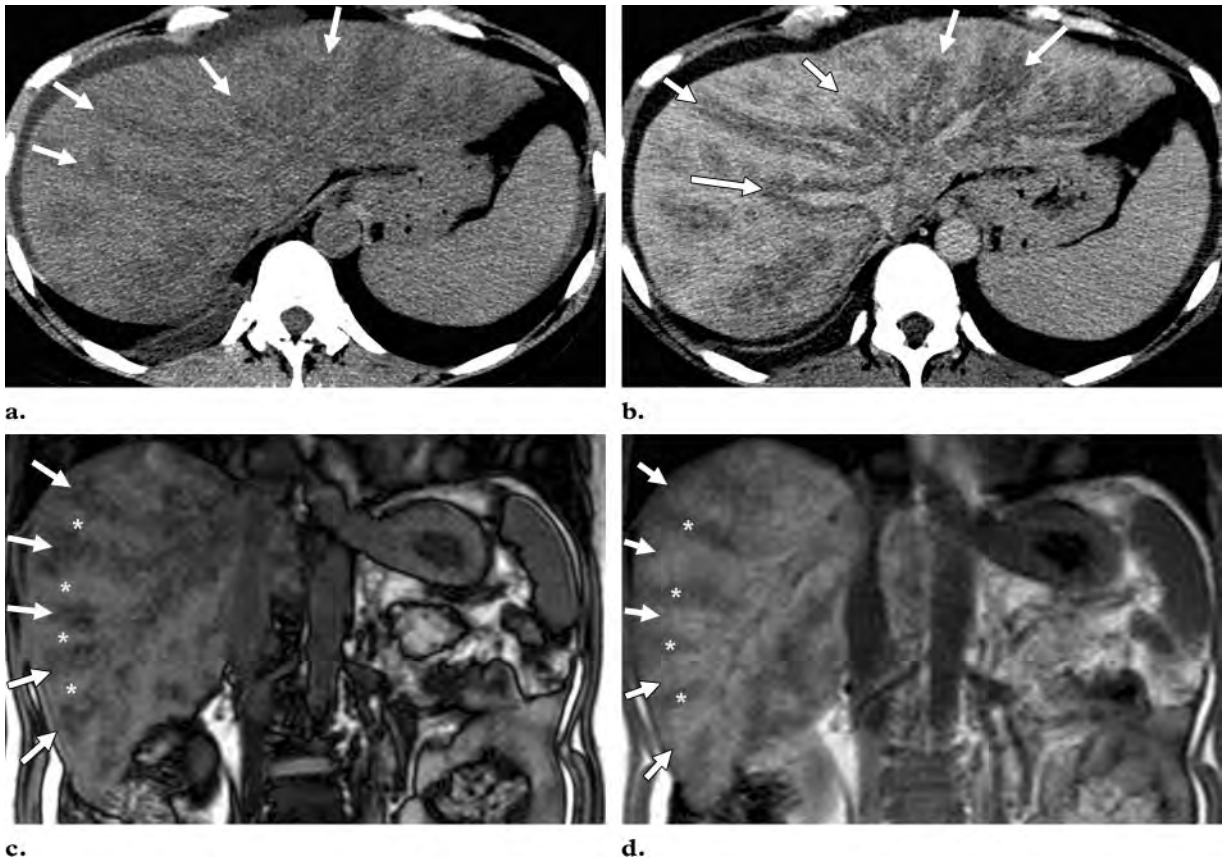

Figure 12. Perivenous fat accumulation in the liver at CT and MR imaging. **(a, b)** Axial unenhanced CT image **(a)** and axial contrast-enhanced equilibrium phase CT image **(b)** show halos of hypoattenuation (<40 HU) that closely surround the hepatic veins (arrows) and that are more visible on **b** than on **a**. The rest of the liver has normal attenuation (63 HU at unenhanced CT). **(c, d)** Coronal T1-weighted GRE MR images. Opposed-phase image **(c)** shows an unequivocal signal intensity loss in the regions that surround the hepatic veins (arrows), which appear slightly hyperintense on the in-phase image (arrows in **d**). This feature helps confirm the presence of fat accumulation. The signal intensity of the normal liver parenchyma (*) in **c** differs from that in **d** because of different window width and level settings.

deposition may be observed within regenerative nodules in some cirrhotic patients; in these cases, the foci of fat accumulation correspond to the fat-containing regenerative nodules. Except for fat deposition in regenerative cirrhotic nodules, the pathogenesis of multifocal fat deposition in the liver is unknown.

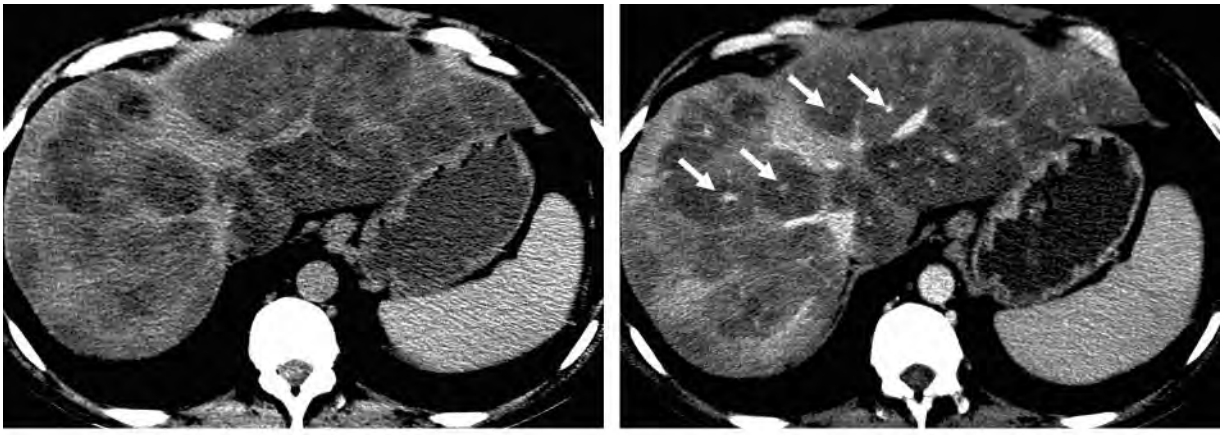

a. b.

Figure 13. Periportal fat accumulation in a patient with a chronic hepatitis B infection. Axial unenhanced **(a)** and contrast-enhanced **(b)** CT images from the late portal venous phase show no morphologic evidence of cirrhosis. Partially confluent halos with hypoattenuation (<40 HU at unenhanced CT) indicative of fat deposition closely surround the portal venous segments (arrows in **b**), with regions of less marked fat deposition bordering the periportal halos and in the periphery of the liver.

Perivascular Deposition

A perivascular pattern of fat deposition in the liver has been described previously (24). This pattern is characterized by halos of fat that surround the hepatic veins, the portal veins, or both hepatic and portal veins (Figs 12, 13). The configuration is tramlike or tubular for vessels with a course in the imaging plane and ringlike or round for vessels with a course perpendicular to the imaging plane. An unequivocal signal intensity loss on opposed-phase images in comparison with that on in-phase images and the lack of a mass effect on the surrounded vessels are indicative of the diagnosis. The pathogenesis of perivascular fat deposition in the liver is unknown.

Subcapsular Deposition

In patients with renal failure and insulin-dependent diabetes, insulin may be added to the peritoneal dialysate during kidney dialysis. This route of insulin administration exposes subcapsular hepatocytes to a higher concentration of insulin than that to which the remainder of the liver is exposed. Since insulin promotes the esterification of free fatty acids into triglycerides, the peritoneal administration of insulin results in a subcapsular pattern of fat deposition, which may be manifested as discrete fat nodules or a confluent peripheral region of fat (49,53). A review of the patient's clinical history in conjunction with the imaging findings should facilitate correct diagnosis.

Differential Diagnosis

The diagnosis of diffuse fat deposition in the liver tends to be straightforward. The differential diagnosis of other patterns of fat deposition is discussed below.

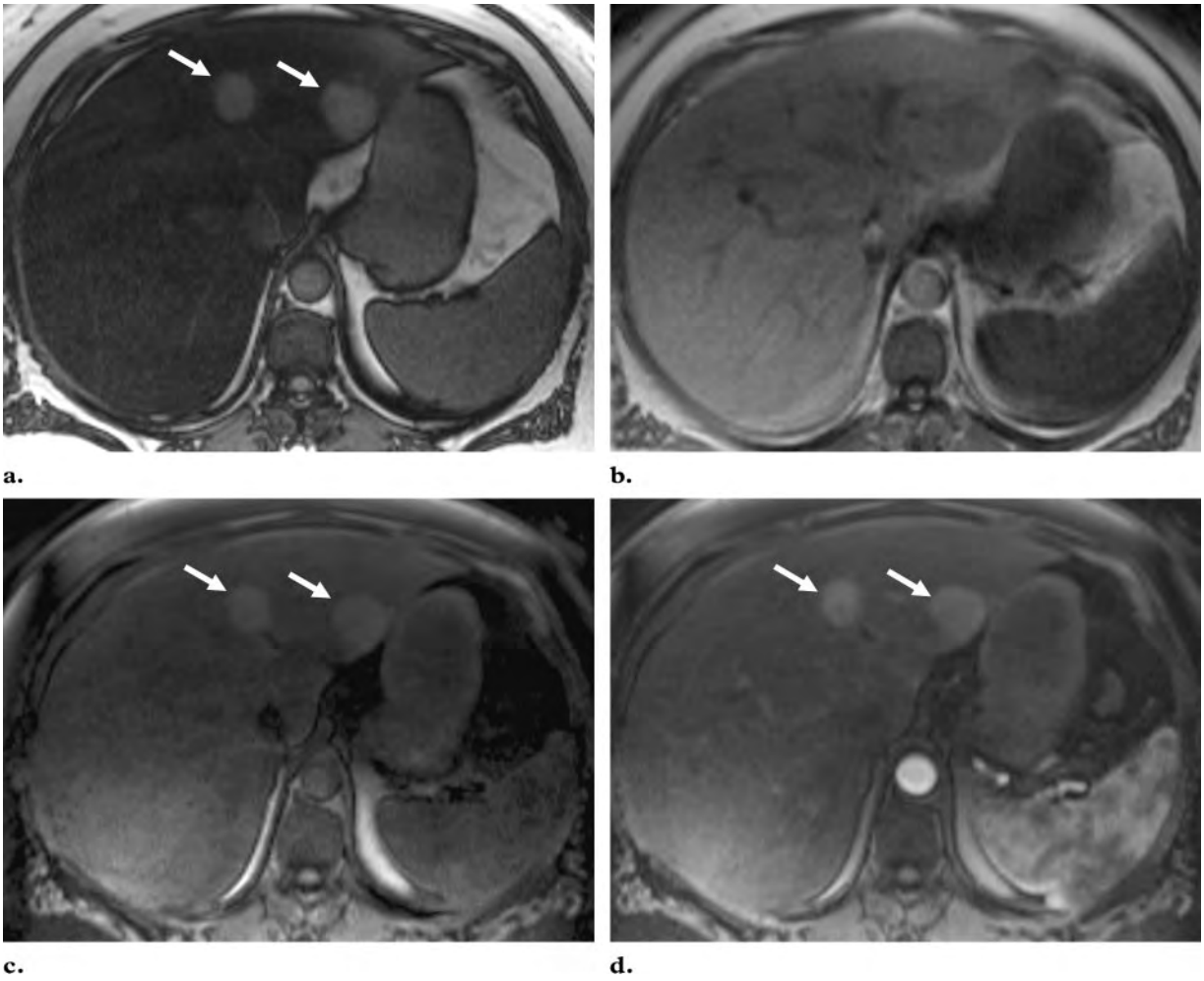

Figure 14. Differentiation of adenoma from fatty deposition in the liver in a woman with a long history of oral contraceptive use. **(a, b)** Axial opposed-phase **(a)** and in-phase **(b)** T1-weighted GRE images show diffuse fat deposition in the liver, indicated by areas with a signal intensity loss on **a** in comparison with **b**. Two round masses in the left lobe of the liver (arrows in **a**) resemble nodular areas of sparing. **(c, d)** Three-dimensional T1-weighted GRE images obtained before **(c)** and during **(d)** the hepatic arterial phase show enhancement of the masses (arrows in **c** and **d**) after the administration of a gadolinium-based contrast agent. The rounded shape of the lesions, as well as their location, which is atypical for regions of fatty liver sparing, are important clues suggestive of tumors. The two masses remained stable in size for several years and most likely are adenomas.

Primary Lesions and Hypervascular Metastases

In general, the differentiation of focal or multifocal fat accumulations from primary hepatic lesions (eg, hepatocellular carcinoma, hepatic adenoma, and focal nodular hyperplasia) or from hypervascular metastases in the liver is not problematic because these lesions exert a mass effect, tend to show vivid or heterogeneous enhancement after contrast agent administration, and may contain areas of necrosis or hemorrhage (Figs 14–16). Infiltrative hepatocellular carcinoma is a notable exception; on CT images, this

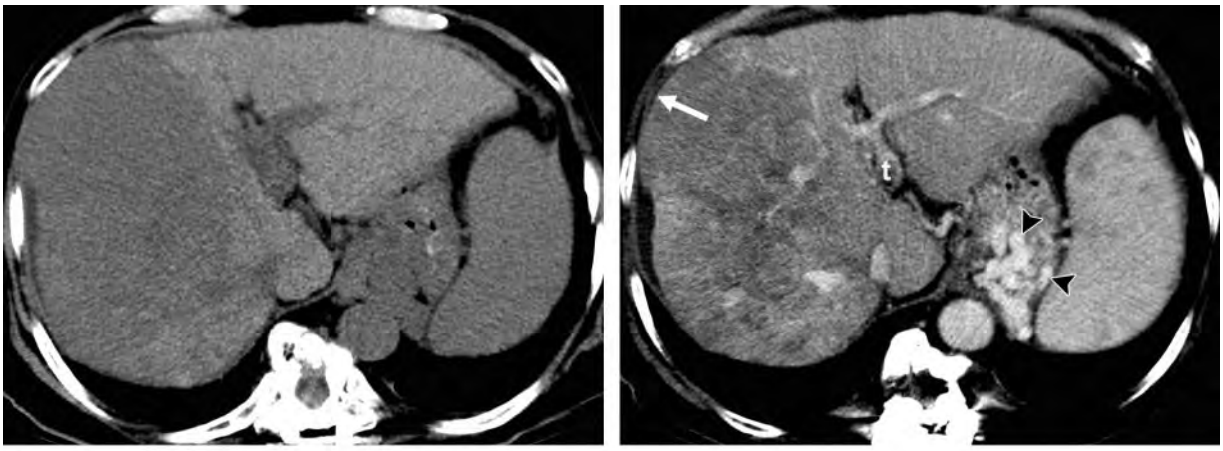

a. b.

Figure 15. Differentiation of hepatocellular carcinoma from fatty deposition in the liver. Axial unenhanced **(a)** and axial contrast-enhanced **(b)** CT images obained during the portal venous phase show a nodular liver contour suggestive of cirrhosis, as well as large gastric varices (arrowheads in **b**). In **b**, the right lobe of the liver appears hypoattenuated in comparison with the left lobe, a finding that could be misinterpreted as evidence of regional fatty liver deposition; however, the mass effect with bulging of the anterolateral border of the right liver lobe (arrow), the mosaic enhancement pattern, and the thrombus *(t)* in the left main portal vein are strongly suggestive of an infiltrative malignancy. This is a case of infiltrative hepatocellular carcinoma.

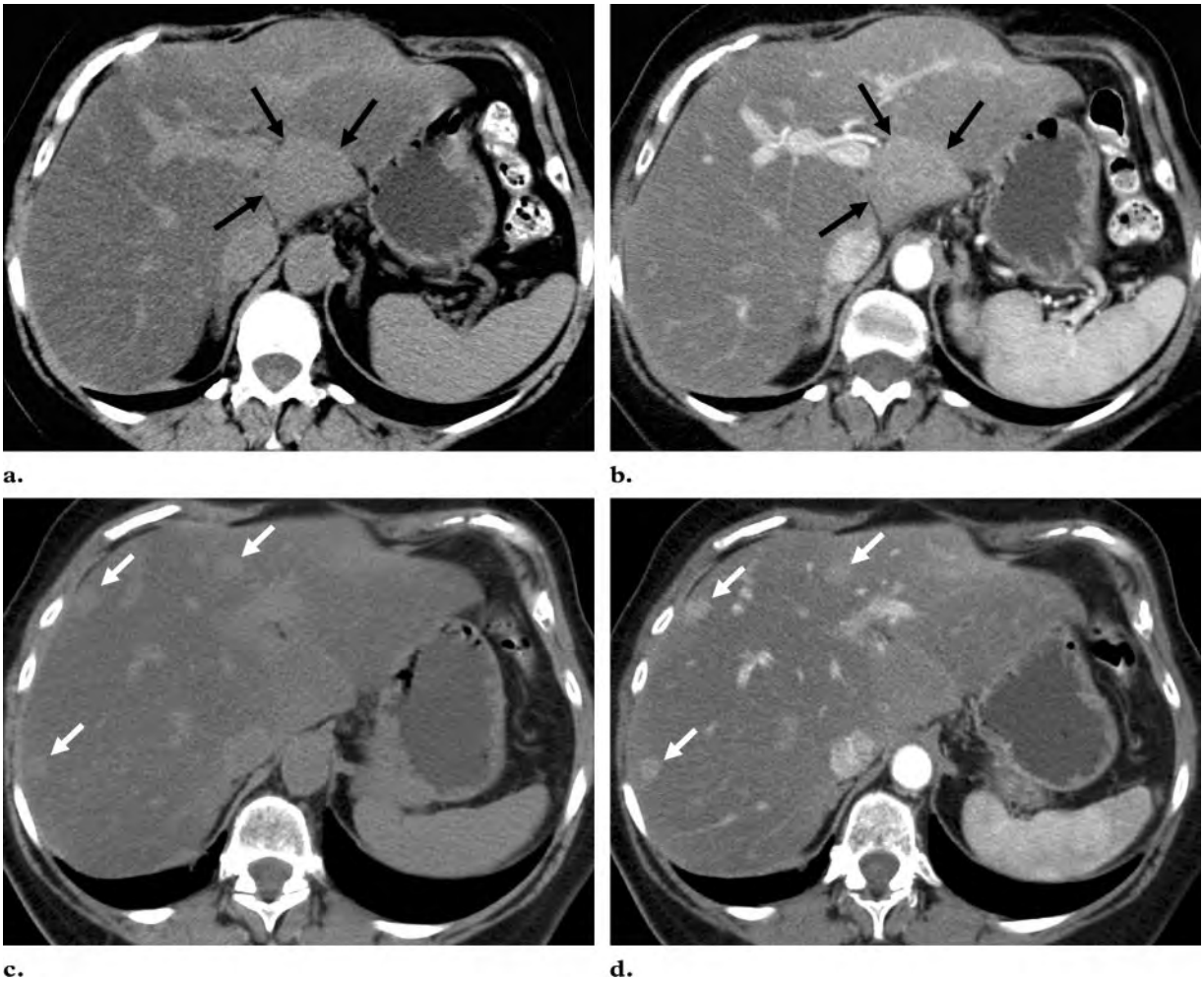

a. b.

c. d.

Figure 16. Differentiation of metastases from fatty liver deposition in a woman undergoing chemotherapy for breast cancer. Axial unenhanced **(a, c)** and contrast-enhanced **(b, d)** CT images (**c** and **d** at a higher level than **a** and **b**) show diffuse fatty deposition in the liver and a geographic pseudolesion at the porta hepatis (arrows in **a** and **b**), a finding that represents focal sparing. Multiple round lesions (arrows in **c** and **d**), which are more vividly enhanced than the liver parenchyma, represent metastases. If unenhanced CT had not been performed, the region of focal sparing on the contrast-enhanced images may have been mistaken for an enhanced hypervascular tumor.

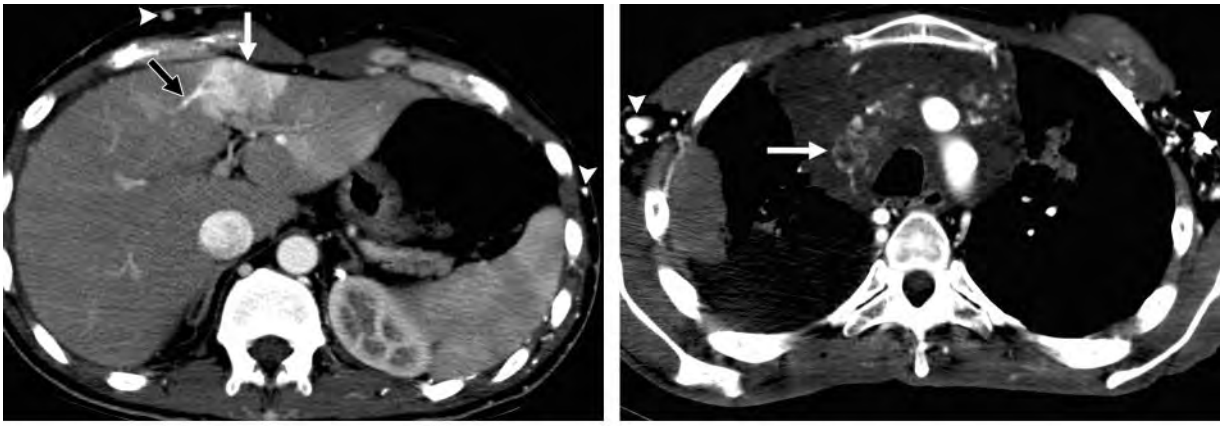

a. b.

Figure 17. Differentiation of superior vena cava syndrome from fatty liver deposition. Axial contrast-enhanced CT images obtained during the arterial phase at the level of the liver **(a)** and the upper mediastinum **(b)** show a hyperattenuated geographic pseudolesion (white arrow in **a**) in segment IV, at the anterior border of the liver, and obstruction of the superior vena cava by a thoracic mass (arrow in **b**). With regard to morphologic features, the pseudolesion resembles a focal area of fatty liver deposition or sparing, but its marked enhancement on early phase images helps confirm that the lesion represents a perfusion abnormality—in this case, one associated with superior vena cava syndrome. Note the large systemic collateral veins (arrowheads in **a** and **b**) and the collateral draining vessel in segment IV (black arrow in **a**).

tumor may exert a minimal mass effect, show little evidence of necrosis, show the same degree of enhancement as the normal liver parenchyma, and closely resemble heterogeneous fat deposition. In our experience, correct diagnosis is usually possible with MR imaging, but the correlation of imaging findings with serum biomarkers may be helpful.

Hypovascular Metastases and Lymphoma

The differentiation of focal or multifocal fat deposition from hypovascular metastases and lymphoma in the liver may be difficult. However, the clinical manifestations and imaging features such as lesion morphology, location, and microscopic fat content usually permit a correct diagnosis. Chemical shift GRE imaging may be necessary to assess the amount of intralesional fat.

Perfusion Anomalies

Perfusion anomalies may resemble fat deposition morphologically but are visible only during the arterial and portal venous phases after contrast

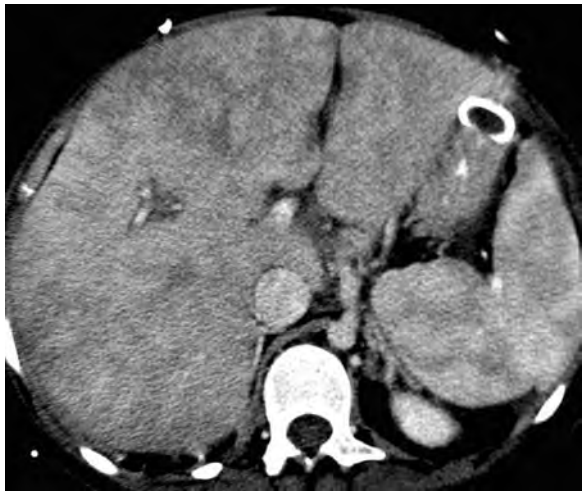

Figure 18. Differentiation of hepatic venous congestion (nutmeg liver) from fatty liver deposition. Axial contrast-enhanced CT image obtained at the level of the liver during the hepatic arterial phase shows irregular areas with low attenuation in the nutmeg pattern, features that could be mistaken for multifocal or geographic fatty liver deposition. However, this pattern was visible only on arterial phase images and early portal venous phase images and not on unenhanced images or images obtained in later phases. A pericardial effusion also was present. Nutmeg liver is a perfusion abnormality that is related to hepatic venous congestion from cardiac disease or other causes.

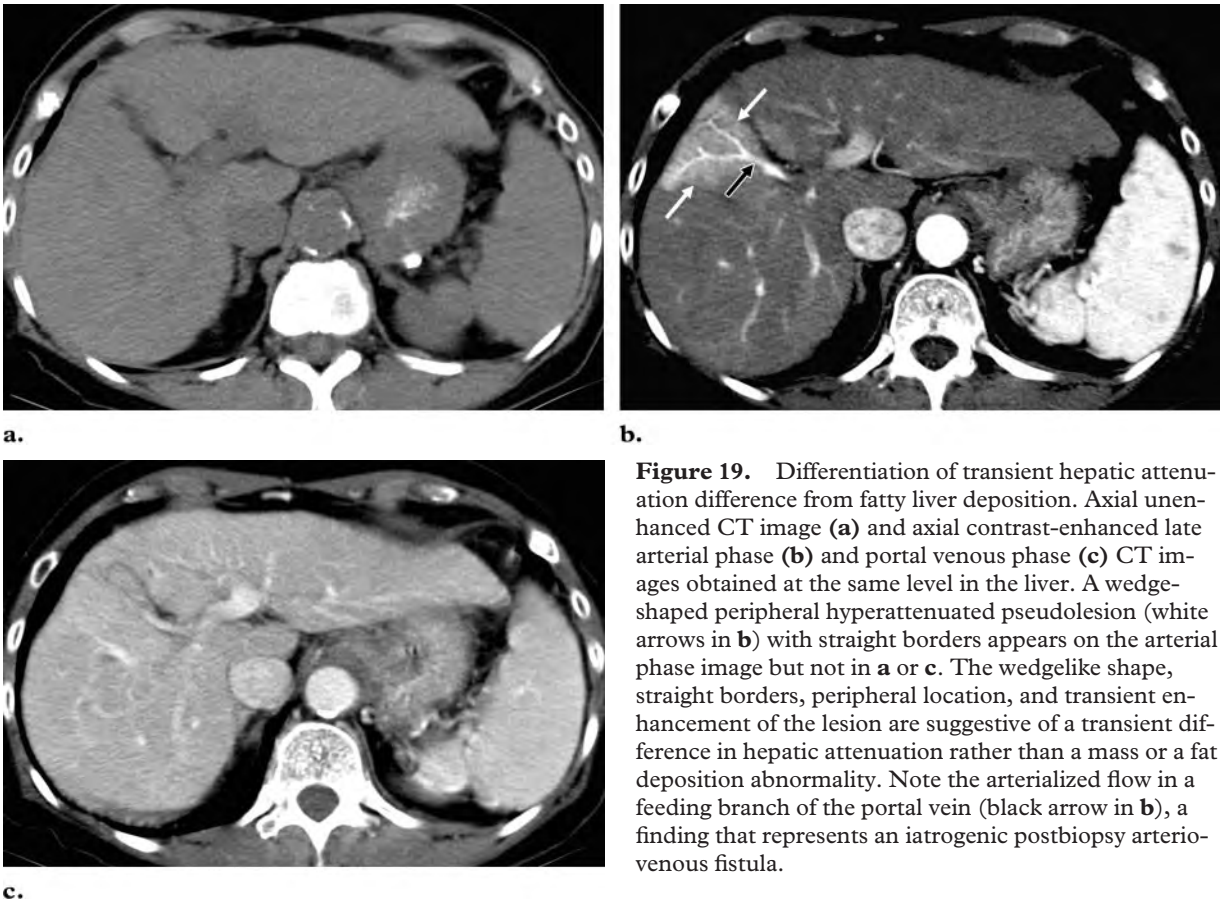

Figure 19. Differentiation of transient hepatic attenuation difference from fatty liver deposition. Axial unenhanced CT image **(a)** and axial contrast-enhanced late arterial phase **(b)** and portal venous phase **(c)** CT images obtained at the same level in the liver. A wedge-shaped peripheral hyperattenuated pseudolesion (white arrows in **b**) with straight borders appears on the arterial phase image but not in **a** or **c**. The wedgelike shape, straight borders, peripheral location, and transient enhancement of the lesion are suggestive of a transient difference in hepatic attenuation rather than a mass or a fat deposition abnormality. Note the arterialized flow in a feeding branch of the portal vein (black arrow in **b**), a finding that represents an iatrogenic postbiopsy arteriovenous fistula.

agent administration. They are not detectable on unenhanced images or equilibrium phase images (Figs 17–19).

Periportal Abnormalities

The US- and CT-based differential diagnosis of periportal fat deposition is broad and includes edema, inflammation, hemorrhage, and lymphatic dilatation (54,55). Edema, inflammation, and lymphatic dilatation tend to affect the portal triads symmetrically. Hemorrhage characteristically involves the portal triads asymmetrically and may be associated with laceration or other signs of injury. None of these entities are associated with microscopic fat. Thus, if chemical shift imaging is performed, a signal intensity loss of perivascular tissue on opposed-phase images permits the correct diagnosis of fat deposition (Fig 20).

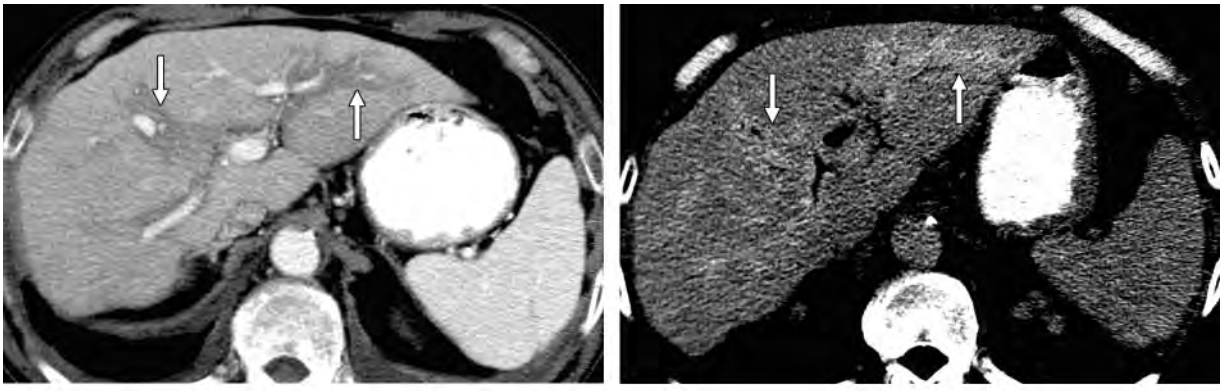

a. b.

Figure 20. Differentiation of periportal inflammation from fatty liver deposition. Axial contrast-enhanced CT images obtained during the portal venous phase **(a)** and the equilibrium phase **(b)**. The hypoattenuated halos (arrows) that surround the portal venous tracts in **a** could be misinterpreted as perivascular fat accumulation, but they retain contrast material and appear hyperattenuated in **b**. Retention of contrast material on delayed images is suggestive of periportal inflammation with transcapillary leakage of the contrast agent into inflamed periportal tissue; perivascular fat deposition would not be expected to retain contrast material. The attenuation of periportal halos should be measured on unenhanced or delayed phase images, if available, to help differentiate periportal fat deposition from edema or inflammation.

Pitfalls

Fat-containing Primary Tumors

Hepatic adenomas, hepatocellular carcinomas, and, rarely, focal nodular hyperplasias may have microscopic fat content (56,57). Hence, a finding of intralesional fat does not help exclude these entities, and clinical findings as well as imaging features such as morphologic structure, mass effect, and enhancement characteristics must be considered (Fig 21).

Low-Attenuation Lesions

A threshold attenuation value of less than 40 HU in the liver at CT is not specific for a finding of fat deposition. For example, ischemic or mucinous metastases or abscesses may manifest low attenuation values (58,59). However, a review of the clinical manifestations and laboratory findings in conjunction with other CT features should lead to the correct diagnosis. If necessary, chemical shift GRE imaging can be performed (Fig 22).

Focal Sparing that Mimics an Enhanced Tumor

If unenhanced images are not obtained, focal sparing in a liver with diffuse fat deposition may mimic an enhanced hypervascular tumor at contrast-enhanced CT. The shape and location of the lesion may permit a correct image-based diagnosis. MR chemical shift imaging can be performed in equivocal cases (Fig 16).

Summary

Fatty liver is a common imaging finding, with a prevalence of 15%–95%, depending on the population. The diagnostic standard of reference is biopsy with histologic analysis, but fat deposition in the liver may be diagnosed noninvasively with US, CT, or MR imaging if established criteria are applied. The most common imaging pattern is diffuse and relatively homogeneous fat deposition. Less common patterns include focal deposition, diffuse deposition with focal sparing, multifocal deposition, perivascular deposition, and subcapsular deposition. These patterns may mimic neoplastic, inflammatory, or vascular conditions, leading to confusion and to unnecessary diagnostic tests and invasive procedures. Assessment of the lesion fat content, location, morphologic features, contrast enhancement, and mass effect usually permits a correct diagnosis. Chemical shift GRE imaging is more reliable than US or CT for assessing intralesional fat and may be necessary when findings are equivocal.

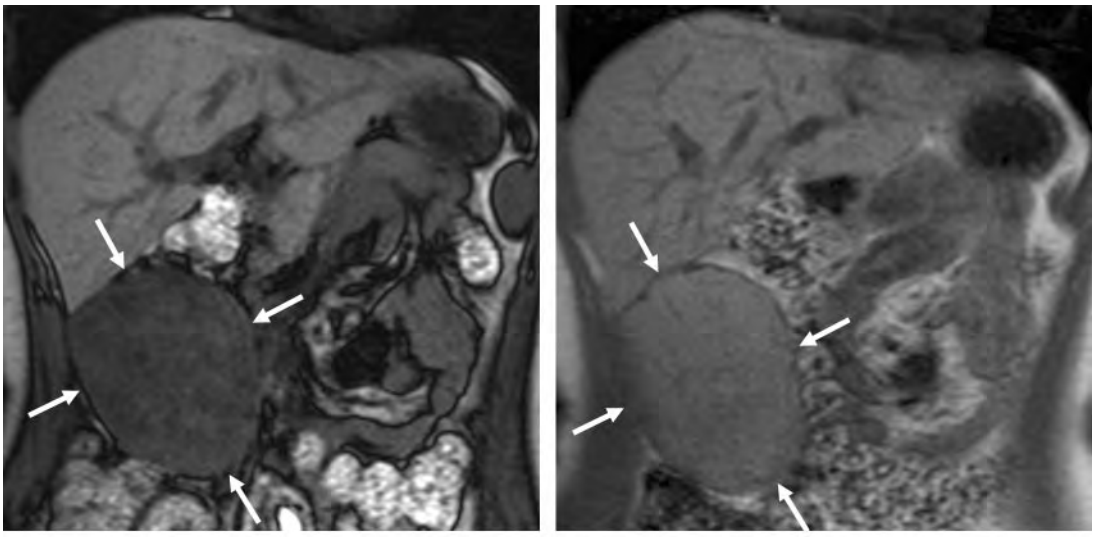

a. b.

Figure 21. Differentiation of a fat-containing tumor from fat deposition in the liver. Coronal T1-weighted GRE MR images show a large mass (arrows) with lower signal intensity on the opposed-phase image **(a)** than on the in-phase image **(b)**, a feature indicative of fat. Vivid arterial enhancement (not shown), the round rather than geographic shape of the lesion, and the mass effect are indicative of a space-occupying lesion rather than fat deposition. The lesion was an exophytic hepatic adenoma.

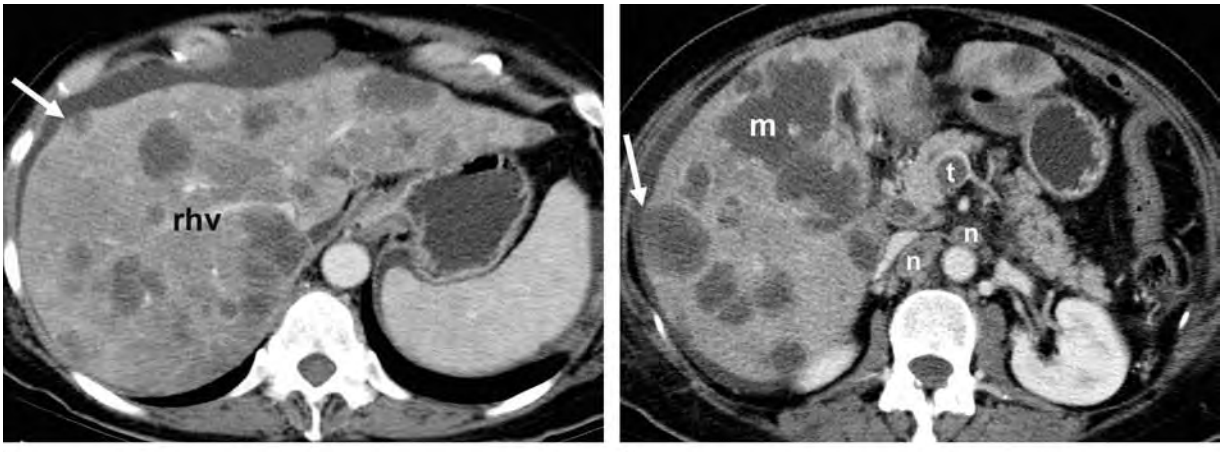

a. b.

Figure 22. Differentiation of metastases from fat deposition in the liver. Axial portal venous phase contrast-enhanced CT images at the level of the right hepatic vein *(rhv)* **(a)** and the pancreatic head **(b)** show innumerable hypoattenuated lesions throughout the liver. Most of the lesions are round or oval, but the largest (*m* in **b**) has a geographic configuration. Because of their low attenuation (<40 HU), the lesions might be mistaken for multifocal fat deposition; however, the mass effect of the lesions, which produces bulging of the liver surface (arrow) and compression of the right hepatic vein, as well as the multiplicity of lesions, their predominant round or oval shape, the thrombus (*t* in **b**) in the superior mesenteric vein, and numerous heterogeneous lymph nodes (*n* in **b**), are suggestive of malignancy. The lesions were identified as hematogenous metastases from pancreatic adenocarcinoma.

References

1. Brunt EM, Tiniakos DG. Pathology of steatohepatitis. Best Pract Res Clin Gastroenterol 2002;16: 691–707.
2. Allard JP. Other disease associations with non-alcoholic fatty liver disease (NAFLD). Best Pract Res Clin Gastroenterol 2002;16:783–795.
3. Eaton S, Record CO, Bartlett K. Multiple biochemical effects in the pathogenesis of alcoholic fatty liver. Eur J Clin Invest 1997;27:719–722.

4. Angulo P. Nonalcoholic fatty liver disease. N Engl J Med 2002;346:1221–1231.
5. Fargion S, Mattioli M, Fracanzani AL, et al. Hyperferritinemia, iron overload, and multiple metabolic alterations identify patients at risk for nonalcoholic steatohepatitis. Am J Gastroenterol 2001; 96:2448–2455.
6. Clark JM, Diehl AM. Nonalcoholic fatty liver disease: an underrecognized cause of cryptogenic cirrhosis. JAMA 2003;289:3000–3004.
7. Scheuer PJ, Lefkowitch JH. Fatty liver and lesions in the alcoholic. In: Liver biopsy interpretation. 6th ed. Philadelphia, Pa: Saunders, 2000; 111–129.
8. Wanless IR, Shiota K. The pathogenesis of nonalcoholic steatohepatitis and other fatty liver diseases: a four-step model including the role of lipid release and hepatic venular obstruction in the progression to cirrhosis. Semin Liver Dis 2004;24: 99–106.
9. Mendez-Sanchez N, Almeda-Valdes P, Uribe M. Alcoholic liver disease: an update. Ann Hepatol 2005;4:32–42.
10. Lefkowitch JH. Morphology of alcoholic liver disease. Clin Liver Dis 2005;9:37–53.
11. Bellentani S, Saccoccio G, Masutti F, et al. Prevalence of and risk factors for hepatic steatosis in Northern Italy. Ann Intern Med 2000;132:112–117.
12. el Hassan AY, Ibrahim EM, al Mulhim FA, Nabhan AA, Chammas MY. Fatty infiltration of the liver: analysis of prevalence, radiological and clinical features and influence on patient management. Br J Radiol 1992;65:774–778.
13. Kammen BF, Pacharn P, Thoeni RF, et al. Focal fatty infiltration of the liver: analysis of prevalence and CT findings in children and young adults. AJR Am J Roentgenol 2001;177:1035–1039.
14. Shen L, Fan JG, Shao Y, et al. Prevalence of nonalcoholic fatty liver among administrative officers in Shanghai: an epidemiological survey. World J Gastroenterol 2003;9:1106–1110.
15. Luyckx FH, Desaive C, Thiry A, et al. Liver abnormalities in severely obese subjects: effect of drastic weight loss after gastroplasty. Int J Obes Relat Metab Disord 1998;22:222–226.
16. Nomura H, Kashiwagi S, Hayashi J, Kajiyama W, Tani S, Goto M. Prevalence of fatty liver in a general population of Okinawa, Japan. Jpn J Med 1988;27:142–149.
17. Joy D, Thava VR, Scott BB. Diagnosis of fatty liver disease: is biopsy necessary? Eur J Gastroenterol Hepatol 2003;15:539–543.
18. Jain KA, McGahan JP. Spectrum of CT and sonographic appearance of fatty infiltration of the liver. Clin Imaging 1993;17:162–168.
19. Saadeh S, Younossi ZM, Remer EM, et al. The utility of radiological imaging in nonalcoholic fatty liver disease. Gastroenterology 2002;123:745–750.
20. Tchelepi H, Ralls PW, Radin R, Grant E. Sonography of diffuse liver disease. J Ultrasound Med 2002;21:1023–1032.
21. Zwiebel WJ. Sonographic diagnosis of diffuse liver disease. Semin Ultrasound CT MR 1995;16:8–15.
22. Piekarski J, Goldberg HI, Royal SA, Axel L, Moss AA. Difference between liver and spleen CT numbers in the normal adult: its usefulness in predicting the presence of diffuse liver disease. Radiology 1980;137:727–729.
23. Limanond P, Raman SS, Lassman C, et al. Macrovesicular hepatic steatosis in living related liver donors: correlation between CT and histologic findings. Radiology 2004;230:276–280.
24. Hamer OW, Aguirre DA, Casola G, Sirlin CB. Imaging features of perivascular fatty infiltration of the liver: initial observations. Radiology 2005;237: 159–169.
25. Pamilo M, Sotaniemi EA, Suramo I, Lahde S, Arranto AJ. Evaluation of liver steatotic and fibrous content by computerized tomography and ultrasound. Scand J Gastroenterol 1983;18:743–747.
26. Yajima Y, Narui T, Ishii M, et al. Computed tomography in the diagnosis of fatty liver: total lipid content and computed tomography number. Tohoku J Exp Med 1982;136:337–342.
27. Ricci C, Longo R, Gioulis E, et al. Noninvasive in vivo quantitative assessment of fat content in human liver. J Hepatol 1997;27:108–113.
28. Johnston RJ, Stamm ER, Lewin JM, Hendrick RE, Archer PG. Diagnosis of fatty infiltration of the liver on contrast enhanced CT: limitations of liver-minus-spleen attenuation difference measurements. Abdom Imaging 1998;23:409–415.
29. Jacobs JE, Birnbaum BA, Shapiro MA, et al. Diagnostic criteria for fatty infiltration of the liver on contrast-enhanced helical CT. AJR Am J Roentgenol 1998;171:659–664.
30. Kreft BP, Tanimoto A, Baba Y, et al. Diagnosis of fatty liver with MR imaging. J Magn Reson Imaging 1992;2:463–471.
31. Rinella ME, McCarthy R, Thakrar K, et al. Dual-echo, chemical shift gradient-echo magnetic resonance imaging to quantify hepatic steatosis: implications for living liver donation. Liver Transpl 2003;9:851–856.
32. Venkataraman S, Braga L, Semelka RC. Imaging the fatty liver. Magn Reson Imaging Clin N Am 2002;10:93–103.
33. Martin J, Puig J, Falco J, et al. Hyperechoic liver nodules: characterization with proton fat-water chemical shift MR imaging. Radiology 1998;207: 325–330.
34. Hussain HK, Chenevert TL, Londy FJ, et al. Hepatic fat fraction: MR imaging for quantitative

measurement and display—early experience. Radiology 2005;237:1048–1055.
35. Rofsky NM, Weinreb JC, Ambrosino MM, Safir J, Krinsky G. Comparison between in-phase and opposed-phase T1-weighted breath-hold FLASH sequences for hepatic imaging. J Comput Assist Tomogr 1996;20:230–235.
36. Thu HD, Mathieu D, Thu NT, Derhy S, Vasile N. Value of MR imaging in evaluating focal fatty infiltration of the liver: preliminary study. RadioGraphics 1991;11:1003–1012.
37. Thomsen C, Becker U, Winkler K, Christoffersen P, Jensen M, Henriksen O. Quantification of liver fat using magnetic resonance spectroscopy. Magn Reson Imaging 1994;12:487–495.
38. Longo R, Ricci C, Masutti F, et al. Fatty infiltration of the liver: quantification by 1H localized magnetic resonance spectroscopy and comparison with computed tomography. Invest Radiol 1993; 28:297–302.
39. Szczepaniak LS, Nurenberg P, Leonard D, et al. Magnetic resonance spectroscopy to measure hepatic triglyceride content: prevalence of hepatic steatosis in the general population. Am J Physiol Endocrinol Metab 2005;288:E462–E468.
40. Choji T. Evaluation of fatty liver changes and fatty degeneration in liver tumors by 1H-MRS [in Japanese]. Nippon Igaku Hoshasen Gakkai Zasshi 1993;53:1408–1414.
41. Gabata T, Matsui O, Kadoya M, et al. Aberrant gastric venous drainage in a focal spared area of segment IV in fatty liver: demonstration with color Doppler sonography. Radiology 1997;203:461–463.
42. Kawamori Y, Matsui O, Takahashi S, Kadoya M, Takashima T, Miyayama S. Focal hepatic fatty infiltration in the posterior edge of the medial segment associated with aberrant gastric venous drainage: CT, US, and MR findings. J Comput Assist Tomogr 1996;20:356–359.
43. Kobayashi S, Matsui O, Kadoya M, et al. CT arteriographic confirmation of focal hepatic fatty infiltration adjacent to the falciform ligament associated with drainage of inferior vein of Sappey: a case report. Radiat Med 2001;19:51–54.
44. Matsui O, Kadoya M, Takahashi S, et al. Focal sparing of segment IV in fatty livers shown by sonography and CT: correlation with aberrant gastric venous drainage. AJR Am J Roentgenol 1995; 164:1137–1140.
45. Rubaltelli L, Savastano S, Khadivi Y, Stramare R, Tregnaghi A, Da Pian P. Targetlike appearance of pseudotumors in segment IV of the liver on sonography. AJR Am J Roentgenol 2002;178:75–77.
46. Itai Y, Saida Y. Pitfalls in liver imaging. Eur Radiol 2002;12:1162–1174.
47. Hoshiba K, Demachi H, Miyata S, et al. Fatty infiltration of the liver distal to a metastatic liver tumor. Abdom Imaging 1997;22:496–498.
48. Fregeville A, Couvelard A, Paradis V, Vilgrain V, Warshauer DM. Metastatic insulinoma and glucagonoma from the pancreas responsible for specific peritumoral patterns of hepatic steatosis secondary to local effects of insulin and glucagon on hepatocytes. Gastroenterology 2005;129:1150, 1365.
49. Sohn J, Siegelman E, Osiason A. Unusual patterns of hepatic steatosis caused by the local effect of insulin revealed on chemical shift MR imaging. AJR Am J Roentgenol 2001;176:471–474.
50. Kroncke TJ, Taupitz M, Kivelitz D, et al. Multifocal nodular fatty infiltration of the liver mimicking metastatic disease on CT: imaging findings and diagnosis using MR imaging. Eur Radiol 2000;10: 1095–1100.
51. Kemper J, Jung G, Poll LW, Jonkmanns C, Luthen R, Moedder U. CT and MRI findings of multifocal hepatic steatosis mimicking malignancy. Abdom Imaging 2002;27:708–710.
52. Monill JM, Martinez-Noguera A, Montserrat E, Sabate JM. Multifocal hepatic steatosis in HIV infection. AJR Am J Roentgenol 1999;172:839.
53. Khalili K, Lan FP, Hanbidge AE, Muradali D, Oreopoulos DG, Wanless IR. Hepatic subcapsular steatosis in response to intraperitoneal insulin delivery: CT findings and prevalence. AJR Am J Roentgenol 2003;180:1601–1604.
54. Lawson TL, Thorsen MK, Erickson SJ, Perret RS, Quiroz FA, Foley WD. Periportal halo: a CT sign of liver disease. Abdom Imaging 1993;18:42–46.
55. Diaz Candamio MJ, Pombo F, Pombo S, Gonzales J, Rodriguez E. Diffuse periportal pathology on CT: differential diagnosis. Presented as scientific exhibit no. 10027 at the European Congress of Radiology, Vienna, Austria, 1999. http://www.ecr.org/Conferences/ECR1999/sciprg/abs/p010027.htm. Accessed August 24, 2004.
56. Mortele KJ, Stubbe J, Praet M, Van Langenhove P, De Bock G, Kunnen M. Intratumoral steatosis in focal nodular hyperplasia coinciding with diffuse hepatic steatosis: CT and MRI findings with histologic correlation. Abdom Imaging 2000;25: 179–181.
57. Prasad SR, Wang H, Rosas H, et al. Fat-containing lesions of the liver: radiologic-pathologic correlation. RadioGraphics 2005;25:321–331.
58. Tang Y, Yamashita Y, Ogata I, et al. Metastatic liver tumor from cystic ovarian carcinomas: CT and MRI appearance. Radiat Med 1999;17:265–270.
59. Halvorsen RA, Korobkin M, Foster WL, Silverman PM, Thompson WM. The variable CT appearance of hepatic abscesses. AJR Am J Roentgenol 1984;142:941–946.

Fatty Liver: Imaging Patterns and Pitfalls

Okka W. Hamer, MD et al

RadioGraphics 2006; 26:1637–1653 • **Published online** 10.1148/rg.266065004 • **Content Code:** GI

Page 1638
The image-based diagnosis of fatty liver usually is straightforward, but fat accumulation may be manifested with unusual structural patterns that mimic neoplastic, inflammatory, or vascular conditions.

Page 1639
Fatty liver may be diagnosed if liver echogenicity exceeds that of renal cortex and spleen and there is attenuation of the ultrasound wave, loss of definition of the diaphragm, and poor delineation of the intrahepatic architecture.

Page 1639
Fatty liver can be diagnosed if the attenuation of the liver is at least 10 HU less than that of the spleen or if the attenuation of the liver is less than 40 HU.

Page 1640
Fatty liver may be present if there is a signal intensity loss on opposed-phase images in comparison with in-phase images, and the amount of hepatic fat present can be quantified by assessing the degree of signal intensity loss.

Page 1641
Imaging findings suggestive of fatty pseudolesions rather than true masses include the following: fat content, location in areas characteristic of fat deposition or sparing, absence of a mass effect on vessels and other liver structures, a geographic configuration rather than a round or oval shape, poorly delineated margins, and contrast enhancement that is similar to or less than that of the normal liver parenchyma.